FATIGUE CRACK GROWTH IN Al-Li/SiC PARTICULATE METAL MATRIX COMPOSITES

I. Sinclair* and J. F. Knott*

A quantitative fractographic analysis of the interaction of SiC particles with fatigue crack path was carried out in a particulate SiC reinforced Al-Li alloy composite. At low stress intensities it was found that SiC particles constituted an unfavourable crack path. At high stress intensities the converse was true, with crack propagation occuring preferentially via the SiC reinforcement. The crack path/SiC particle interaction appeared to be K_{max} dependent. These results were rationalised in terms of interparticle spacing and scale of the crack tip stress field as stress intensity increased.

INTRODUCTION

Silicon carbide reinforced aluminium alloys have been recognised as potentially attractive engineering materials due to their enhanced specific strength and modulus over conventional aluminium alloys. The fracture toughness and ductility of aluminium alloys is however generally reduced by inclusion of SiC particles (e.g. McDanels, (1)). The fatigue resistance of Al-SiC composites is commonly comparable to, if not better, than that of unreinforced aluminium alloys, although long crack, high ΔK growth rates usually compare less favourably with those of monolithic alloys, in keeping with the lower toughness of the composites (e.g. Davidson (2)).

Important information on the fatigue resistance of Al/SiC MMC's may be obtained from the examination of the influence of SiC on the crack path (e.g. in

*Dept. Material Science & Metallurgy, Cambridge University, England

developing crack tip 'shielding' effects). Although many papers have qualitatively described the fractography of these materials (e.g. Yau and Mayer (3)), few have applied quantitative fractographic analysis to their findings (Shang *et al.* (4)). It has been observed by Shang *et al.* (4) and Kumai *et al.* (5) that SiC particles consitute a less favourable propagation path at low/threshold stress intensities, than at high stress intensity levels. This paper outlines the results of a quantitative fractographic analysis of fatigue crack propagation in SiC particulate reinforced, high strength aluminium-lithium alloy, 8090, undertaken to quantify this observation.

EXPERIMENTAL

Materials. Co-spray deposited (White *et al.* (6)) Al-Li alloy 8090, nominally containing 8 Vol% SiC particulate (F600 grit, av. size approx 13μm) was produced by Alcan Int., Banbury, as 20mm diameter extruded bar. The following heat treatment was carried out; 540°C/30minutes solution treatment, cold water quench, 2% stretch, age 150°C/40 hours. This material was then machined into SEN bend specimens (W=12mm, B=10mm, S=15mm). The extrusion process produces an aligned SiC distribution as shown in fig 1. The matrix consisted of fine fibrous grains approx. 5μm × 30μm aligned in the extrusion direction. Typical properties were supplied as; 0.2%P.S. 480 MPa, T.S. 530 MPa, E=100 GPa, E.f. 2.6%.

Mechanical Testing and Fractography. Computer controlled, load shedding and constant load, increasing ΔK tests were carried out on a 60 kN Mand servohydraulic machine at room temperature, in laboratory air. R-ratios (P_{max}/P_{min}) of 0.1 and 0.3 were employed. Crack lengths were monitored using the D.C.P.D. method. Fracture surfaces were examined using a Camscan S4 SEM operated at 30 kV. Optical fractography was carried out on polished centre section profiles of specimens which had been previously vacuum impregnated with epoxy resin.

Quantitative Fractography. A Seescan image analysis system was used to measure fractographic quantities from the mid-section profile specimens described above. The system allowed for measurement of the length of the crack profile (L_t), length of crack profile through SiC particles (l_i) and measurement of local volume fraction of SiC in the region immedately behind the fracture profile ($[V_V]_{SiC.local}$), see diagram 2. Quantitative metallographic analysis of the SiC distribution was also undertaken using the Seescan system.

RESULTS

Figure 3 shows crack growth rate results and includes a scatter band for data published on unreinforced 8090 tested under similar conditions (Knowles and King (8)). Fatigue crack growth resistance is comparable at low to intermediate stress intenisties. At higher ΔK levels growth rates in the composite tend towards higher values, in keeping with an expected lower fracture toughness in the composite. The

maximum value of K_{max} prior to fracture was estimated to be approx. 23 MPa$\sqrt{m}$.

Figures 4 and 5 show typical fatigue fracture surfaces over the measured ΔK range, and overload fracture. Transgranular crack growth is observed across the range of ΔK, with little evidence of the intergranular failure often observed in Al-Li alloys (Baker *et al.* (7)). SiC particles are observed more frequently on the fatigue surface as the stress intensity increases. The monotonic fracture surface consists of large dimples (10-20μm) associated with SiC particles with intervening areas of fine dimples (2-4μm) and some regions of shear failure. Crack profile examination showed various crack/ particle interactions; decohesion (particularly associated with corners of the particles), cracking through the SiC and deflection around the particles. Although cracking and decohesion were observed more frequently at higher stress intensities, neither mechanism clearly predominated.

The results obtained from quantitative analysis of the crack path were used to deduce the crack path preference index (or crack path fraction) of SiC along the fatigue fracture surface, G_{SiC}, as defined by (Underwood (9)):

$$G_{SiC} = \frac{\Sigma\,(l_i)}{L_t}$$

This index was divided by the measured local volume fraction of SiC to produce a crack path parameter, Γ_{SiC}, i.e.

$$\Gamma_{Sic} = \frac{G_{SiC}}{[V_v]_{SiC.local}}$$

This normalization was carried out to remove the scatter in results due to the local fluctuations in volume fraction (to be expected in even an entirely random distribution). From this parameter it is possible to deduce the degree to which the actual cracking process occurs preferentially through the SiC particles, i.e. a random crack path would produce a value of unity.

The measured values of Γ_{SiC} (averaged over a projected crack length of 450 μm) are plotted against ΔK and K_{max} in figs 6 &7. The results show a broad scatter band which is assumed to be due to the statistically small sampling areas for each ΔK level. As a general trend it can be seen that the crack path preference of the SiC particles changes from being unfavourable at low stress intensities, to becoming a preferred crack path at higher levels. Although scatter in Γ_{SiC} prevents clear inferral of the effect of R-ratio on path preference, it can be seen that the higher R-ratio tends to give greater Γ_{SiC} values for a given ΔK level (fig 6). Plotting these results against K_{max} shifts the scatter bands together (fig 7). Linear regression on both data sets indicates a $K_{max} \sim 13$MPa$\sqrt{m}$ at the point where Γ_{SiC} equals unity. The average length of crack through a SiC particle (l_i) was measured as 3.8μm and was not

measured as 3.8μm and was not found to change with the value of K.

Quantitative analysis of the SiC distribution indicates a mean free path between particles of around 40μm in the longitudinal plane (i.e. that of the crack profile). The mean intercept length of the SiC was 3.6μm in the transverse direction, and 6.7μm in the longitudinal direction.

DISCUSSION

The effect of R-ratio would suggest the contribution of SiC to the crack path is K_{max} dependent, and therefore arises from static loading behaviour, although a larger number of profile samples would be required to qualify this completely. From the observation that the average length of intersection with each SiC particle does not change significantly with K_{max}, it may be deduced that the increase in path preference arises from an increase in number of SiC particles along the crack as stress intensity levels increase. This behaviour may be rationalised in terms of two possible events when a propagating fatigue crack approaches a reinforcing particle: The first is that the particle remains intact (does not fracture or decohere) causing the crack to be deflected. This may be considered due to the influence of a high modulus inclusion on the local stress distribution (Padkin *et al.* (10), Tirosh and Tetelman (11)). Secondly, the particle may fail monotonically under the stresses ahead of the crack and link up with the main crack front. Results from the present work could be then modelled by considering the SiC particles strong enough, and sufficiently well bonded to the matrix, to withstand the stresses required to deflect an approaching crack before experiencing the very high stresses close to the crack tip. However as the stress intensity levels rise, the very highly stressed region, within which stresses are high enough to cause the SiC to fail, becomes larger than the particle spacing. When this occurs the particles become a favourable crack path. In terms of the value of Γ_{SiC} it can be seen that if the process of the interaction of each particle is invariant with K (at least in the contribution to crack length through each particle), and the "cracking length" is approximately the same as the mean intercept length of the particles in the crack direction (i.e. $\bar{l}_i$ = 3.8 μm and mean intercept length (transverse) = 3.6 μm) then the point were Γ_{SiC} = 1 represents a situation where the effects of deflection and cracking are balanced. Although no in-depth analysis of the appropriate crack tip plastic zone/stress field size and particle distribution parameters have been considered here, it may be noted that, at K_{max} = 13MPa$\sqrt{m}$, the extent of the plain strain plastic zone (given by Rice (12)) is approx. 110 μm. The size of the highly strained region at the crack tip (McMeeking (13)) is around 3.5 μm. The measured mean free path between SiC particles was measured as approximately 45 μm, falling between these two crack tip parameters.

CONCLUSIONS

(1) Fatigue crack propagation resistance of this material is broadly comparable with

conventional 8090 aluminium.

(2) SiC particles are avioded by fatigue cracks growing at low stress intensities, but preferencially sought out by the crack at high stress intensities.

(3) The change in crack path preference of the SiC particles may be qualitatively explained in terms of the scale of the crack tip stress field, and the particle distribution.

REFERENCES

(1) McDanels, D.L., Met. Trans. A, Vol.16A, 1985, p1105

(2) Davidson, D.L., Tech. Report, N00014-85-0206, (Southwest Research Inst., San Antonio, Texas), 1988

(3) Yau, S.S., Mayer, G., Mat. Sci. Engng. Vol.82, 1986, p45

(4) Shang, J.R., Yu, W. and Ritchie, R. O., Mat. Sci. Engng. Vol.102A, 1988, p181

(5) Kumai, S., King, J.E. and Knott, J.F., submitted to Mat. Sci. Engng, 1989

(6) White, J., Hughes, R., Willis, T.C., and Jordan, R.M., J. Physique, Vol.48, 1987, C3-347

(7) Baker, C. *et al.*, Eds. "Al-Li Alloys III", Institute of Metals, London, England, 1985

(8) Knowles, D. and King, J.E., to be published in "Fatigue 90"

(9) Underwood, E.E., "Fracture Mechanics: Microstructure and Micromechanics", Eds. Nair, S.V. *et al.*, ASM, 1989

(10) Padkin, A.J., Brereton, M.F. and Plumbridge, W.J., Mat. Sci. Tech., Vol.3, 1987, p217

(11) Tirosh, J. and Telelman, A.A., Int. J. Frac., Vol.12, 1976, p187

(12) Rice, J.R., Mech. Phys. Solids, Vol.22, 1974, p17

(13) McMeeking, R.M., Mech. Phys. Solids, Vol 25, 1977, p357

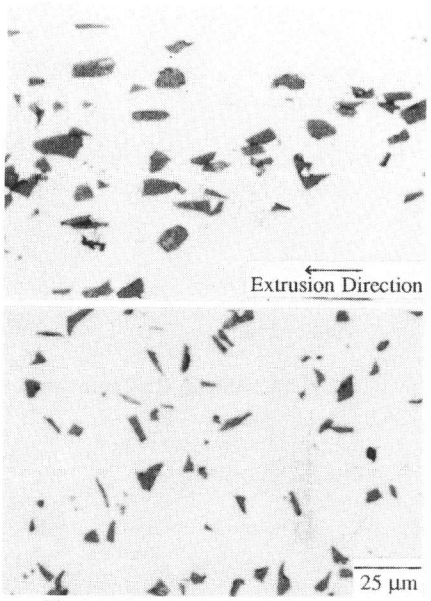

Fig. 1 (a) Longitudinal and (b) transverse microstucture of composite.

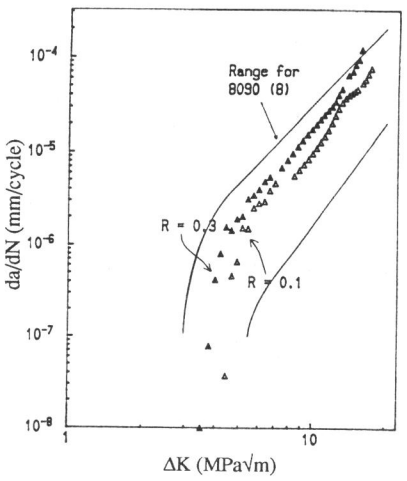

Fig. 3 Fatigue crack growth rates in composite at R = 0.1 and 0.3.

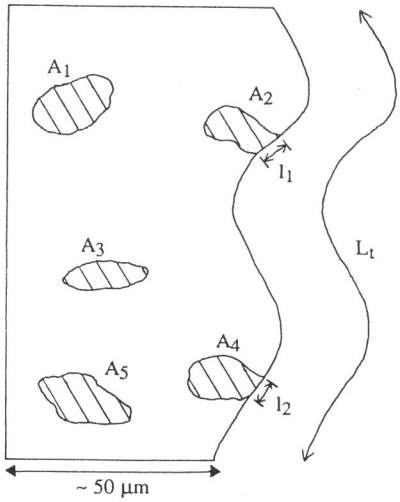

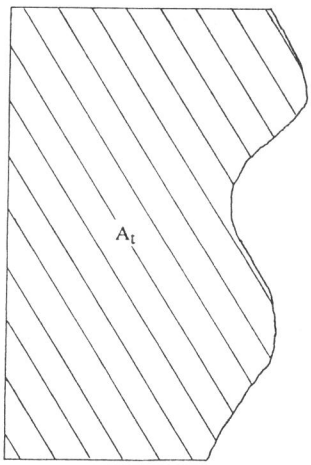

$$[V_v]_{SiC.local} = \left(\Sigma A_i\right) / A_t$$

Fig. 2 Schematic illustration of profile and local volume fraction measurements.

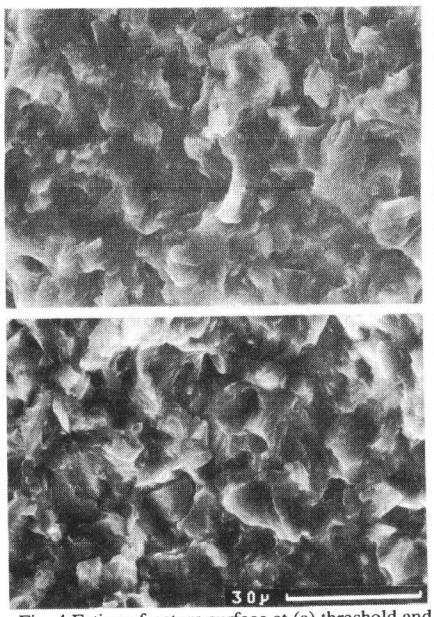

Fig. 4 Fatigue fracture surface at (a) threshold and (b) $\Delta K \sim 6$ MPa$\sqrt{m}$.

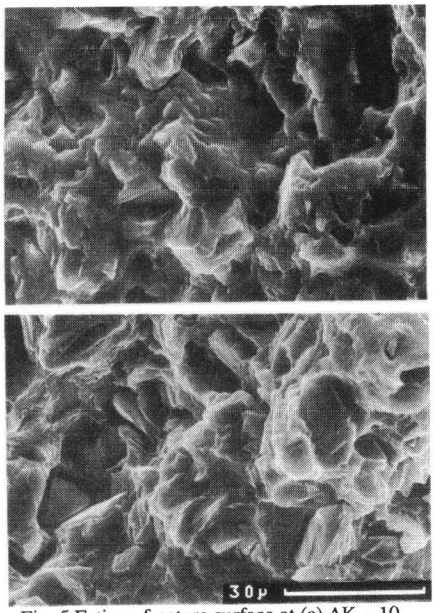

Fig. 5 Fatigue fracture surface at (a) $\Delta K \sim 10$ MPa$\sqrt{m}$ and (b) monotonic fracture.

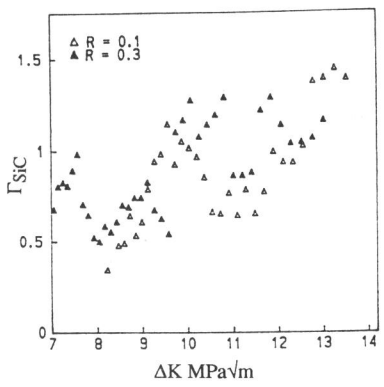

Fig. 6 Variation of Γ_{SiC} with ΔK.

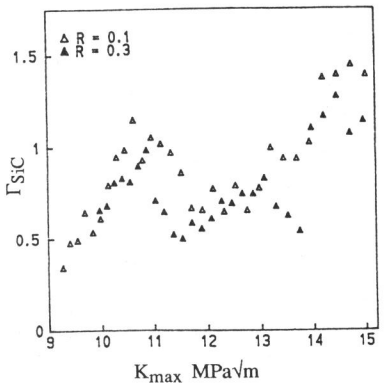

Fig. 7 Variation of Γ_{SiC} with K_{max}.